

Improvement of Magnetic Field for Near-Field WPT System Using Two Concentric Open-Loop Spiral Resonators

Mohamed Aboualalaa¹, Graduate Student Member, IEEE, Islam Mansour, Adel Barakat², Member, IEEE, Kuniaki Yoshitomi, Member, IEEE, and Ramesh K. Pokharel³, Member, IEEE

Abstract—This letter introduces two concentric open-loop spiral resonators (OLSRs) that are used to improve magnetic field for nonradiative wireless power transfer (WPT) systems. OLSRs are fed through metal–insulator–metal (MIM) capacitive coupling using a 50- Ω microstrip transmission line. First, a single OLSR is designed and implemented for WPT, then two OLSRs are used instead of a single OLSR to emphasize the surface current on the spiral resonators. Therefore, it helps to intensify the electromagnetic field in order to get a high transmission distance or higher efficiency. The proposed WPT system operates at 438.5 MHz with a measured power transfer efficiency (PTE) of 70.8% at a transmission distance of 31 mm and a design area of 576 mm². An equivalent circuit of the proposed WPT system is presented as a heuristic approach to show the electrical behavior of the WPT system.

Index Terms—Capacitive coupling feeding, charging distance, near-field wireless power transfer (WPT), open-loop spiral resonator (OLSR), power transfer efficiency (PTE).

I. INTRODUCTION

WIRELESS power transfer (WPT) technologies have received much more attention during the last decade due to their effectiveness in wireless charging for a wide range of electronic appliances [1]–[8]. To transmit power between two points without a physical link, conventional WPT systems use two coils [9]—one coil is a transmitter (Tx) and the other is a receiver (Rx)—that generate an induced current from the received power. Two main factors control the performance of the WPT scheme, power transfer efficiency (PTE) and transmission range (d). PTE refers to how much power received by the rechargeable device compared to the power transmitted by the transmitter; while transmission range indicates the longest distance between Tx and Rx at

Manuscript received June 18, 2020; accepted August 7, 2020. This work was supported in part by Progress 100 (Invitation program for top global researchers) and in part by the VLSI Design and Education Center (VDEC), University of Tokyo, in collaboration with Keysight Corporations. (Corresponding author: Mohamed Aboualalaa.)

Mohamed Aboualalaa is with the Microstrip Department, Electronics Research Institute, Giza 12622, Egypt, and also with the Graduate School of Information Science and Electrical Engineering, Kyushu University, Fukuoka 819-0385, Japan (e-mail: mohamed.ali@ejust.edu.eg).

Islam Mansour is with the Electrical Engineering Department, Shoubra Faculty of Engineering, Benha University, Cairo 11629, Egypt (e-mail: islam.mansour@feng.bu.edu.eg).

Adel Barakat, Kuniaki Yoshitomi, and Ramesh K. Pokharel are with the Graduate School of Information Science and Electrical Engineering, Kyushu University, Fukuoka 819-0385, Japan (e-mail: yoshitomi@ed.kyushu-u.ac.jp; pokharel@ed.kyushu-u.ac.jp).

Color versions of one or more of the figures in this letter are available online at <http://ieeexplore.ieee.org>.

Digital Object Identifier 10.1109/LMWC.2020.3016136

which the receiver can receive power with acceptable PTE. Several studies were carried out to improve these parameters (PTE and d) [10]–[14]. Many research studies proposed using ferrite materials for increasing PTE. In [11], a novel structure of a ferrite core is used to concentrate the magnetic field. On the other hand, several techniques used strong coupled intermediate resonators. In [12], magnetic resonant couplers are utilized as intermediate materials between Tx and Rx to increase PTE. A wideband four-coil strongly coupled magnet resonance system is introduced in [13]. A substrate-integrated spiral resonator is presented in [15] to solve the size issue in the intermediate coupled resonators. While a hybrid technique which merges ferrite into the intermediate materials is applied in [14] by using repeater coils with an inserted ferrite plates in the repeaters in addition to putting ferrite plates in transmitting and receiving coils. The previously mentioned techniques improved the coupling for WPT systems. However, there are many obstacles with these methods; for example, using strong coupled intermediate resonator is not practical due to fixing problems for the intermediate resonators. Regarding applying ferrite materials with WPT, frequency and temperature limitations can restrict using ferrite materials because after a few megahertz (MHz) the losses increase dramatically; besides, the permeability of ferrite materials changes with temperature changes leading to instability problems. A heavy weight of the ferrite also makes its applications are so limited. Recently, higher frequencies have been suggested to enable efficient WPT with compact size receiver [16], [17].

In this letter, a double spiral open-loop resonator is used to strengthen the magnetic field and then coupling between Tx and Rx. A circuit model for the proposed WPT is also discussed in this letter. The model is executed using Agilent Advanced Design System (ADS) simulator. While the electromagnetic (EM) simulation results are carried out using a 3-D full-wave EM simulator [Ansys high-frequency structure simulator (HFSS)].

II. PROPOSED NEAR-FIELD WPT SYSTEM

First, a single three-turn circular-shaped printed spiral coil with an inner radius of 3 mm and a width of 0.55 mm is designed and implemented as a band stop filter (BSF) to check its capability in power decoupling by putting it below two-port microstrip line as shown in Fig. 1(a). It yielded good results, where most of the power is coupled to the spiral coil; which means it can be used to transfer the power wirelessly by coupling if another symmetrical coil (acts as a Rx) is put in a vicinity of this coil (acts as Tx) with a certain separation distance between them. By introducing another spiral coil [Spiral coil (2)] with 180° angular spatial rotation with the

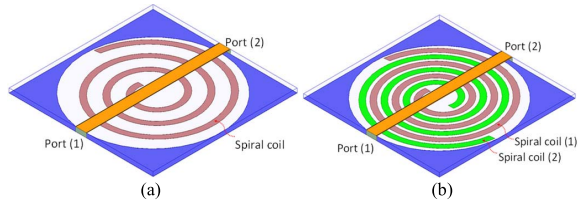


Fig. 1. BSF structure of (a) three turns single coil and (b) three turns double coil.

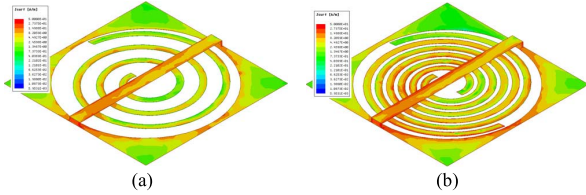


Fig. 2. Surface current distribution of BSF of (a) single coil and (b) double coil.

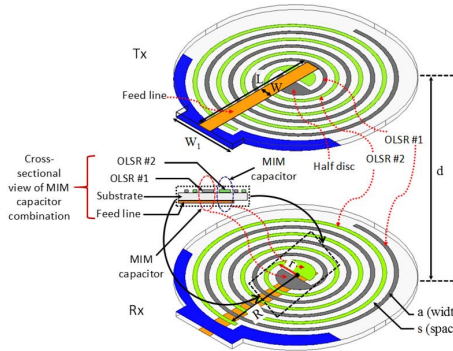


Fig. 3. OLSR WPT geometry. $W = 2$ mm, $W_1 = 10$ mm, $L = 18$ mm, $R = 12.6$ mm, $r = 3$ mm, $a = 0.55$ mm, and $s = 0.95$ mm.

original spiral coil [Spiral coil (1)] as illustrated in Fig. 1(b), the surface current is strengthened at the same operating frequency. Thus, it can also increase the coupling between Tx and Rx. This, in turn, gives a large transmission distance between Tx and Rx. Fig. 2 shows a comparison of the surface current distribution for a single and a double coil, it is clear that surface current concentration is higher in the case of a double coil than that of a single spiral coil due to increasing the number of turns which have current distribution in the same direction. Using a single coil with increasing the number of turns and minimizing the gap between the turns, it can also focus the surface current. However, the operating frequency will decrease as well that makes the WPT design size is small at the emerging low frequency. Thus, Tx–Rx coupling still has the same value without an improvement. Until now, it is not verified that these coils can operate as a WPT system with a high transmission distance. To verify that, therefore, a WPT system using the configuration of the two spiral coils is introduced as shown in Fig. 3. Metal–insulator–metal (MIM) capacitive coupling feeding is used, each spiral coil represents an inductor, and it is excited through one MIM capacitor to transfer most of the excitation power from the feed line into one terminal of the spiral inductor. While the other terminal is an open circuit and this is why it is called open-loop spiral resonator (OLSR) where the new emerging resonator includes the series combination between the MIM capacitor and the spiral-loop inductor. Hence, the spiral inductor (1) becomes OLSR #1 and the spiral inductor (2) turns to OLSR #2.

Fig. 3 shows a cross-sectional of the combination of the MIM capacitor. MIM capacitor is composed of two copper

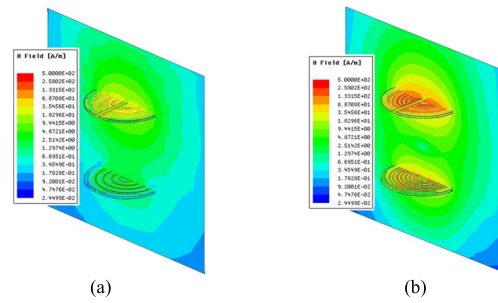


Fig. 4. Magnetic field coupling between Tx and Rx. (a) Magnetic field for a single OLSR. (b) Magnetic field for a double OLSR.

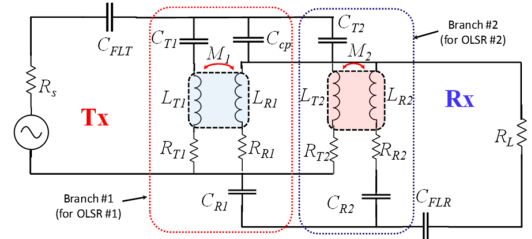


Fig. 5. Equivalent circuit model; circuit parameters values are $C_{FLT} = C_{FLR} = 0.11$ pF, $C_{T1} = C_{R1} = 11$ pF, $L_{T1} = L_{R1} = 2.2$ μ H, $C_{T2} = C_{R2} = 12.1$, $L_{T2} = L_{R2} = 2.6$ μ H, $R_S = R_L = 50$ Ω , $M_1 = 35.8$ nH, $M_2 = 37.6$ nH, and $R_{T1} = R_{T2} = R_{R1} = R_{R2} = 6$ Ω .

plates with a confined substrate between them, one plate is a half disk and the second metallic plate is the intersection area of the feed line with this metallic half disk as shown in Fig. 3. The feed line has dimensions of 2 mm \times 18 mm with 50- Ω impedance. The proposed OLSRs are designed on Rogers Duroid RO3003 substrate with a dielectric constant (ϵ_r) of 3, substrate thickness (h) of 0.76 mm, copper thickness (t) of 0.0017 mm, and a dielectric loss tangent ($\tan\delta$) of 0.0013. The geometrical parameters of the proposed WPT design are also shown in Fig. 3. From the simulation results of the magnetic coupling fields between Tx and Rx, in Fig. 4, it is clear that the magnetic coupling in case of double OLSR [see Fig. 4(b)] is higher than that of a single OLSR [see Fig. 4(a)].

III. EQUIVALENT CIRCUIT MODEL

The equivalent circuit model of the proposed WPT system is revealed in Fig. 5. There are two branches in the equivalent circuit. Each branch is concerned with a single OLSR and it shows how the coupling is represented between Tx and Rx for a single OLSR.

For example, the gray OLSR (OLSR #1 for Tx/Rx) as shown in Fig. 3, the feed line excites the OLSR through MIM capacitive coupling (C_{T1} and C_{R1}). Where subscripts T and R represent Tx and Rx, respectively. C_{T1} and C_{R1} are connected in series with an inductance L_{T1} and L_{R1} , respectively. These inductances represent OLSR self-inductance. The loss resistances for OLSRs are R_{T1} and R_{R1} for Tx and Rx, respectively. In the same manner, the second OLSR (OLSR #2) is represented. Where OLSR parameters take subscript 1 and 2 for OLSR #1 and OLSR #2, respectively. R_S and R_L represent the source and load resistances, respectively, which physically mean the port impedance for the Tx/Rx of the proposed WPT system. The preliminary values of the equivalent circuit parameters are calculated from microwave theory as follows.

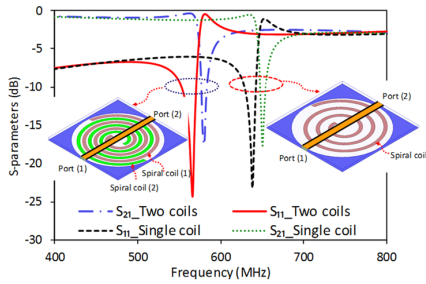


Fig. 6. Reflection and transmission coefficients of a single and double coil BSF.

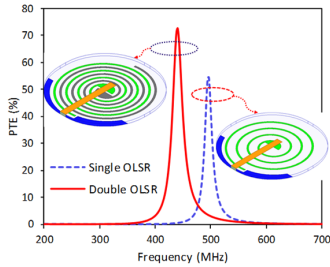


Fig. 7. PTE of a single and double OLSR.

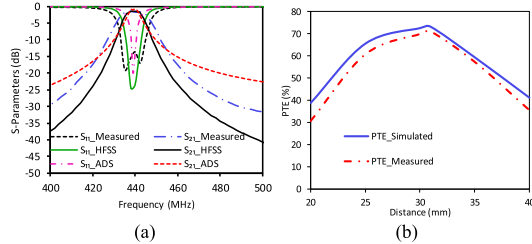


Fig. 8. (a) Reflection and transmission coefficients of the proposed WPT. (b) PTE versus transmission distance for the proposed double OLSR.

- 1) Starting with the feed line, it has a small length ($l = 18 \text{ mm} \ll \lambda/4 \cong 95 \text{ mm}$), so it acts as a capacitor (C_{FL}).
- 2) MIM capacitance (C_T or C_R) is calculated by determining the values of substrate permittivity (ϵ_r), substrate height (h) which represents the distance between the two plates of the capacitor, and the shared area (A) between the feed line and the half disk.
- 3) OLSRs can be represented by a series RL circuit. The initial values of the inductance (L_T or L_R) are calculated like an open circuit stub that has a certain length and width with resistance losses of R_T and R_R . While mutual inductance (M_1 and M_2) is calculated from the impedance matrix using HFSS EM simulator where $M = \text{imag}(Z_{21}) / (2\pi \times \text{freq})$.
- 4) The capacitive coupling represented in C_{cp} has a small value, and it is adjusted to get the desired S-parameters as in HFSS simulator.

To simplify the equivalent circuit model, we ignored the small value of the coupling between the two resonators (OLSR #1 and OLSR #2). The ultimate values of the equivalent circuit parameters are summarized in Fig. 5. The simulated results of the S-parameters (S_{11} , S_{12} , S_{21} , and S_{22}) of the proposed equivalent circuit using Agilent ADS circuit simulator are compared with the measured results as shown in Fig. 8(a).

IV. RESULTS AND DISCUSSION

A BSF performance of a single and a double spiral coil, with a number of coil turns of three turns, is illustrated

TABLE I
WPT PERFORMANCE COMPARISON WITH RECENTLY PUBLISHED LETTERS

Ref.	Frequency (MHz)	\sqrt{A} (mm)	d (mm)	d/\sqrt{A}	η_{measured} (PTE %)	FoM*	FoM**
[4]	433	45	22	0.49	87.9	0.43	0.21
[6]	300	21	25	1.19	73	0.86	1.03
[8]	300/675	20	17	0.85	80/73	0.68/0.62	0.58/0.53
This work	438.5	24	31	1.29	70.8	0.92	1.18

$$FoM^* = \frac{PTE \times d}{\sqrt{A}} \quad [6] \quad \text{and} \quad FoM^{**} = \frac{\eta \times d^2}{(A_{TX})^{\frac{1}{3}} \times (A_{RX})^{\frac{1}{3}}} \quad [18], \quad \eta_{\text{measured}}(\%) = 10^{(P_r - P_t + P_{cl})/10} \times 100, \quad A \text{ is WPT area, } d \text{ is transmission distance and cable losses } (P_{cl}) = 0.22 \text{ dB}$$

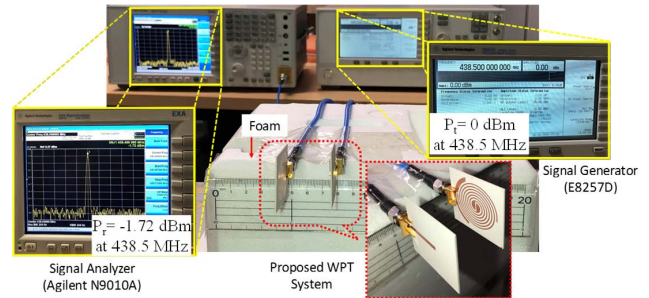


Fig. 9. Measurement setup that is used to get the experimental results.

in Fig. 6. The operating frequency is controlled by the number of the coils' turns. Also, a comparison between the PTE for a single and double OLSR is illustrated in Fig. 7. The simulated results show the enhancement in PTE in double OLSR. The proposed double OLSR WPT system operates at 440 MHz with PTE of 72.5% at a transmission distance of 31 mm. While for a single OLSR, PTE is 56% at 487 MHz at the same transmission distance. This shift in the operating frequency between single and double OLSRs comes from the emerging additional mutual coupling between the two resonators (OLSR #1 and OLSR #2) in the case of using double OLSRs which decreases the operating frequency. Fig. 8(a) displays the simulated S-parameters results (reflection coefficient and transmission coefficient) using HFSS and Agilent ADS as well as the measured results. Fig. 8 shows that the optimal charging distance is 31 mm at the highest PTE, after that PTE starts to decline with decreasing the coupling between the Tx/Rx. PTE also reduces at lower values of the charging distances because the overcoupling result in splitting the efficiency curve to give maximum PTE both sides of at the operating frequency; while PTE becomes lower at the operating frequency. The measured PTE is decreased to 70.8% at 438.5 MHz, there is also a slight shift in the experimental frequency due to the fabrication and soldering tolerance. A ratio of the transmission distance (d) to design size (A) can be used to evaluate the design performance. Table I is a comparison between the proposed WPT design and recently published WPT systems. The experimental setup is shown in Fig. 9.

V. CONCLUSION

Double concentric OLSRs are proposed for WPT applications. MIM capacitive coupling is used to increase the OLSR launched power for higher transmission distance. The measured PTE for the proposed OLSRs WPT is 70.8% at 438.5 MHz at a transmission distance of 31 mm. The proposed WPT system is designed and implemented and there is a good agreement between simulated and experimental results.

REFERENCES

- [1] M. M. Falavarjani, J. Rashed-Mohassel, and M. Shahabadi, "Design and implementation of compact WPT system using printed spiral resonators," *Electron. Lett.*, vol. 50, no. 2, pp. 110–111, Jan. 2014.
- [2] M. Rozman *et al.*, "Smart wireless power transmission system for autonomous EV charging," *IEEE Access*, vol. 7, pp. 112240–112248, Aug. 2019.
- [3] A. B. Islam, S. K. Islam, and F. S. Tulip, "Design and optimization of printed circuit board inductors for wireless power transfer system," *Circuits Syst.*, vol. 4, no. 2, pp. 237–244, 2013.
- [4] J. Wang *et al.*, "A conformal split-ring loop as a self-resonator for wireless power transfer," *IEEE Access*, vol. 8, pp. 911–919, Jan. 2020.
- [5] L. L. Pon, S. K. A. Rahim, C. Y. Leow, M. Himdi, and M. Khalily, "Displacement-tolerant printed spiral resonator with capacitive compensated-plates for non-radiative wireless energy transfer," *IEEE Access*, vol. 7, pp. 10037–10044, Jan. 2019.
- [6] S. Hekal, A. B. Abdel-Rahman, H. Jia, A. Allam, A. Barakat, and R. K. Pokharel, "A novel technique for compact size wireless power transfer applications using defected ground structures," *IEEE Trans. Microw. Theory Techn.*, vol. 65, no. 2, pp. 591–599, Feb. 2017.
- [7] L. L. Pon, C. Y. Leow, S. K. A. Rahim, A. A. Eteng, and M. R. Kamarudin, "Printed spiral resonator for displacement-tolerant near-field wireless energy transfer," *IEEE Access*, vol. 7, pp. 172055–172064, 2019.
- [8] R. Sharaf, A. B. Abdel-Rahman, A. S. Abd El-Hameed, A. Barakat, S. Hekal, and A. Allam, "A new compact dual-band wireless power transfer system using interlaced resonators," *IEEE Microw. Wireless Compon. Lett.*, vol. 29, no. 7, pp. 498–500, Jul. 2019.
- [9] A. Kurs, A. Karalis, R. Moffatt, J. D. Joannopoulos, P. Fisher, and M. Soljacic, "Wireless power transfer via strongly coupled magnetic resonances," *Science*, vol. 317, no. 5834, pp. 83–86, Jul. 2007.
- [10] S. B. Lee and I. G. Jang, "Coil layout optimization for maximizing the power transfer efficiency of wireless power transfer systems with multiple transmitter coils," *IEEE J. Emerg. Sel. Topics Power Electron.*, vol. 8, no. 3, pp. 2672–2681, Sep. 2020.
- [11] M. Wang, J. Feng, Y. Shi, and M. Shen, "Demagnetization weakening and magnetic field concentration with ferrite core characterization for efficient wireless power transfer," *IEEE Trans. Ind. Electron.*, vol. 66, no. 3, pp. 1842–1851, Mar. 2019.
- [12] M. J. Chabalko, J. Besnoff, and D. S. Ricketts, "Magnetic field enhancement in wireless power with metamaterials and magnetic resonant couplers," *IEEE Antennas Wireless Propag. Lett.*, vol. 15, pp. 452–455, Jul. 2016.
- [13] W. Zhou, S. Sandeep, P. Wu, P. Yang, W. Yu, and S. Y. Huang, "A wideband strongly coupled magnetic resonance wireless power transfer system and its circuit analysis," *IEEE Microw. Wireless Compon. Lett.*, vol. 28, no. 12, pp. 1152–1154, Dec. 2018.
- [14] C. Cheng *et al.*, "Load-independent wireless power transfer system for multiple loads over a long distance," *IEEE Trans. Power Electron.*, vol. 34, no. 9, pp. 9279–9288, Sep. 2019.
- [15] X. Q. Lin, Z. Y. Kang, F. Cheng, and Y. Fan, "A compact substrate integrated spiral resonator for wireless power transfer," in *IEEE MTT-S Int. Microw. Symp. Dig.*, Suzhou, China, Jul. 2015, pp. 1–3.
- [16] L. Li, H. Liu, H. Zhang, and W. Xue, "Efficient wireless power transfer system integrating with metasurface for biological applications," *IEEE Trans. Ind. Electron.*, vol. 65, no. 4, pp. 3230–3239, Apr. 2018.
- [17] F. L. Cabrera and F. R. de Sousa, "Backscatter efficiency modeling of inductive links applied to wireless power transfer systems," *IEEE Trans. Microw. Theory Techn.*, vol. 66, no. 5, pp. 2386–2392, May 2018.
- [18] P. Chen, H. Yang, R. Luo, and B. Zhao, "A tissue-channel transcutaneous power transfer technique for implantable devices," *IEEE Trans. Power Electron.*, vol. 33, no. 11, pp. 9753–9761, Nov. 2018.